Appendix

A1. Comparison between node-wise and layer-wise depth compensation algorithm

In the present study, we have used a node-wise depth-compensation weight function, $\mathbf{M}_{\text{node}}$, as given in equation (12) in the paper, for the brain atlas-based DC-DOT. It is a moderate modification from the original layer-wise depth-compensation weight matrix, $\mathbf{M}_{\text{layer}}$, given by Niu et al. (2010). Specifically, the original layer-wise compensation was introduced for a perfectly-layered homogeneous model, where a vector of layer-wise singular values of the optical sensitivity matrix, $\mathbf{A}$, was computed and then reversed as a compensation weight function to counterbalance the severe decay of depth-variant optical sensitivity. A parameter γ was induced to control the compensation power. In general, the optimal γ value depends on specific probe geometry and optical properties of the tissue. However, the layer-wise compensation cannot be directly used on the heterogeneous head mesh since it does not have a perfectly-layered structure. Knowing that $\mathbf{M}_{\text{layer}}$ has a pseudo-exponential form, therefore, we have modified the compensation weight function or matrix by using a direct exponential term, as given in equation (12), which consists of the exact depth of each node with a compensation power, η. It is noted that both node-wise and layer-wise matrixes, $\mathbf{M}_{\text{node}}$ and $\mathbf{M}_{\text{layer}}$, offer a similar depth compensation trend to overcome the severe loss of measurement sensitivity as the depth increases.

In order to examine and confirm the performance of this modification, we compared DC-DOT images reconstructed with $\mathbf{M}_{\text{node}}$ and $\mathbf{M}_{\text{layer}}$ through computer simulations based on a semi-infinite, homogeneous model of tissue. The medium had a background absorption coefficient of $\mu_a = 0.1$ cm^{-1} and reduced scattering coefficients of $\mu_s' = 10$ cm^{-1}, respectively. A rectangle optode array, as shown in Fig. 1(a) in this paper, was placed on the surface of the tissue, providing a total of 71 measurements at the 1st nearest source-detector separation of 1.6 cm and a total of 98 measurements at the 2nd nearest source-detector separation of 3.6 cm. A single-voxel absorber ($2 \times 2 \times 1$ mm^3) with $\mu_a = 0.3$ cm^{-1} and $\mu_s' = 10$ cm^{-1} was embedded under the center of the optode array. The depth of the absorber was varied from 0.2 cm to 3.0 cm at a step of 0.1 cm.

The performance of $\mathbf{M}_{node}$ and $\mathbf{M}_{layer}$ was evaluated based on positional error (PE), which was defined as the absolute distance from the actual location of the absorber to its corresponding center in the reconstructed image. Following the method described by Niu et al. (2010), PE was studied as a function of depth and compensation power, γ for $\mathbf{M}_{layer}$ and η for $\mathbf{M}_{node}$. An identical regularization parameter α = 0.01 was used for both methods. As shown in fig. A1, the results clearly demonstrate that at γ= 1.3 (dash line in Fig. A1a) in layer-wise compensation and η = 3.2 (dash line in Fig. A1b) in node-wise compensation, the PE outputs can be minimized or optimized across depths of 0 to 3 cm. At the optimal compensation power (γ = 1.3 and η = 3.2), the node-wise compensation indeed has slightly smaller positional errors than the original layer-wise compensation.

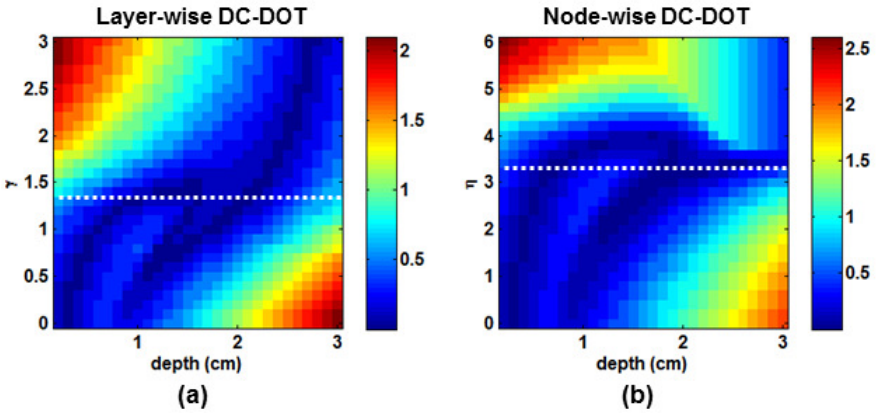

Fig. A1 Dependence of positional error (PE, in cm) of the reconstructed images on absorber depth and depth compensation power (γ and η) by using depth-compensation weight matrix of (a) $\mathbf{M}_{layer}$ and (b) $\mathbf{M}_{node}$. The dash line in each graph indicates the optimal compensation power, i.e., γ= 1.3 in (a) and η = 3.2 (b).

A2. Comparison among Con-DOT, SVR-DOT and DC-DOT

Based on the same homogeneous model, we also compared the performance of Con-DOT, SVR-DOT and DC-DOT using $\mathbf{M}_{layer}$ and $\mathbf{M}_{node}$. Specifically, the depth of the absorber was varied from 0.4 cm to 2.4 cm at a step of 0.2 cm; an identical regularization parameter α = 0.01 was used for all the DC-DOT methods. A spatial regularization factor χ = 0.1 was used for SVR-DOT; the optimal values of compensation power determined by Fig. A1 were used for DC-DOT. Figure A2 below shows cross-sectional images (y = 0) of

the absorber reconstructed at respective depths using Con-DOT, SVR-DOT and DC-DOT, respectively. This figure demonstrates that while Con-DOT and SVR-DOT start to break down when the absorber was at 1.2 cm and 1.6 cm, respectively, both layer-wise and node-wise DC-DOT are able to locate the absorber correctly up to 2-cm depth and approximately at 2.4-cm depth with a few millimeters of PE.

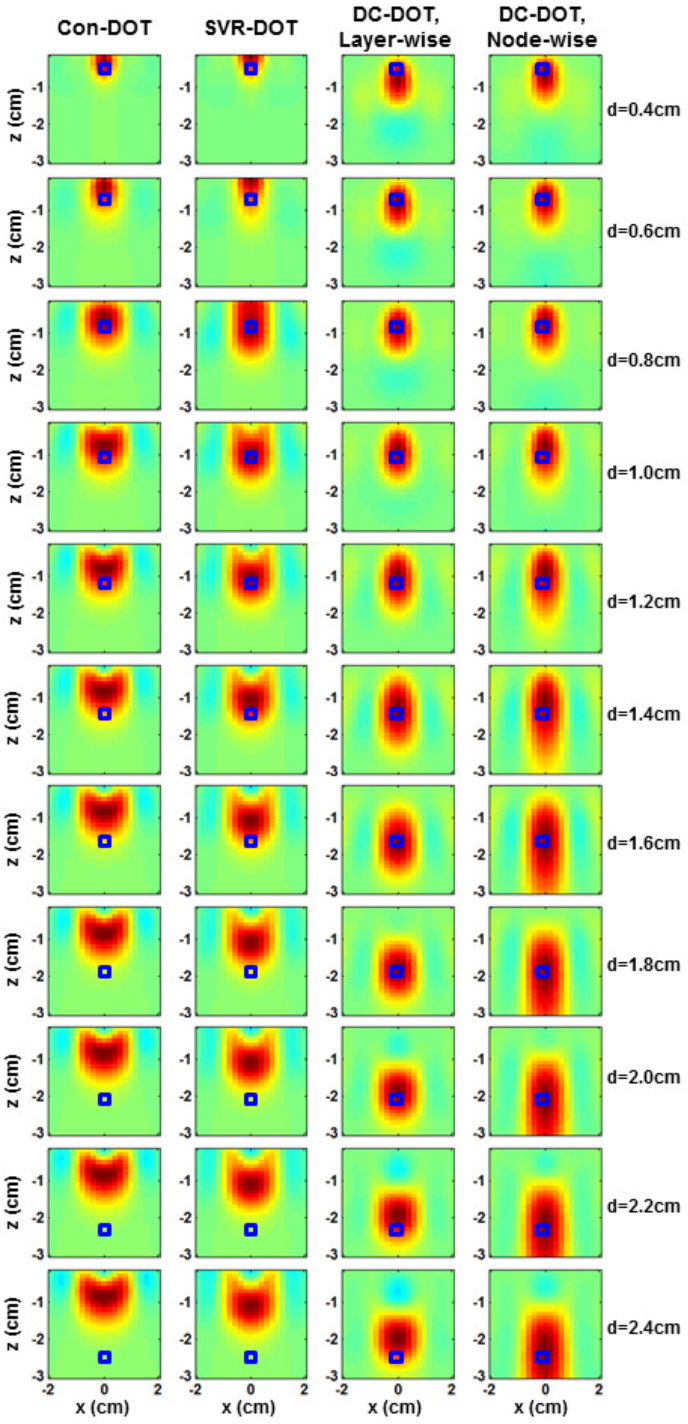

Fig. A2 Reconstructed images of a single-voxel absorber (vertical profile at y = 0) using Con-DOT, SVR-DOT and DC-DOT. The small blue square in each graph indicates the actual location of the absorber.

However, we notice from this figure that the cross-sectional images reconstructed by node-wise DC-DOT are significantly lengthened in z-direction when the absorber approaches larger depths (>1.0 cm). Our interpretation of this phenomenon is that only the 1st and 2nd nearest source-detector separations were used in image reconstruction, limiting the depth specification of the method in the deeper field. This problem can be partially solved by using multiple source-detector separations in image reconstruction, as demonstrated in Fig. A3. On the other hand, the lengthened pattern of reconstructed DC-DOT images implies and hints the weakness of the node-wise depth compensation method. In order words, eq. (12) needs to be refined in order to improve the spatial resolution along depth. Indeed, the elongated character of DC-DOT images by using node-wise depth compensation may be the underlying cause of imperfect *t*-maps stretched into the "deeper" brain region, as seen in Figs. 6-8. One alternative solution to this problem is to resume layer-wise DC-DOT by appropriately defining and segmenting specific layers according to human head curvatures, instead of utilizing flat layers previously used for a homogeneous model. This approach will take place in our future studies.

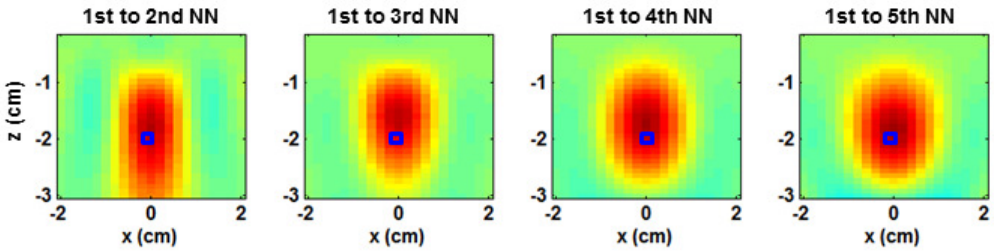

Fig. A3 Reconstructed images of a single-voxel absorber (cross-section at y = 0) at a depth of 2.0 cm using node-wise DC-DOT and variable source-detector separations. The small blue square in each graph indicates the actual location of the absorber.